Materials Chemistry and Physics xxx (2016) 1–5

Contents lists available at ScienceDirect

Materials Chemistry and Physics

journal homepage: www.elsevier.com/locate/matchemphys

Materials science communication

Chemical, textural and structural evolution of $Ni_{1-x}O$ nanoparticles upon isothermal air heating

Dominique Larcher [a, b, *], Kévin Croué [a, b], Matthieu Courty [a, b]

[a] Laboratoire de Réactivité et Chimie des Solides, Université de Picardie Jules Verne, CNRS UMR 7314, 33 rue Saint Leu, 80039, Amiens, France
[b] Réseau sur le Stockage Electrochimique de l'Energie (RS2E), FR CNRS 3459, France

HIGHLIGHTS

- Nanometric (4 nm) monodisperse $Ni_{1-x}O$ (7% Ni^{3+}) particles are air-heated at 320 °C.
- Saturation in oxygen (4% Ni^{3+}) and maximum in strains are reached simultaneously.
- Strains and excess oxygen are then released upon further isothermal heating.
- Final loss of oxygen requires transient creation of new crystallite boundaries.
- Final loss of oxygen requires the transient increase in % Ni^{3+}.

ARTICLE INFO

Article history:
Received 28 August 2015
Received in revised form
26 January 2016
Accepted 10 February 2016
Available online xxx

Keywords:
Sintering
Inorganic compounds
Defects
Oxides

ABSTRACT

The isothermal air heating (320 °C) of monolithic nanometric $Ni_{1-x}O$ (~4 nm, 7% Ni^{3+}) particles results in their sintering and concomitant loss of excess oxygen, leading to almost stoichiometric monolithic larger particles (~7 nm, 0.5% Ni^{3+}). By coupling crystallographic, thermal, textural and chemical analyses of the powders along heating, we could demonstrate that their evolutions in structure, texture and chemical composition are intimately linked and non-monotonous. First, while the particles/crystallites progressively coalesce and increase in size, their level of crystallographic strains increases until a saturation step in oxygen is reached (8 h). With time, this excess in oxygen is then progressively released, as well as the associated strains, and then the particles size and specific surface area stabilize (13 h). Beyond 13 h, the level of strains still monotonously decreases while a transient gain in oxygen/weight and a temporary decrease in crystallite size are observed before the final monolithic powder is produced (34 h).

1. Introduction

Beyond an apparent simple formula/composition, NiO is a prosperous material with a large variety of applications as catalytic [1], gas sensor [2,3], electrochromic [4,5], p-type semi-conductor [6] and magnetic [7] materials and in many energy conversion devices (water electrolysis [8], DSCs photocathodes [9], battery electrodes [10], capacitors [11–13], Li–O_2 cells [14] and Molten Carbonate Fuel Cells (MCFC) [15]), owing to its electronic structure and ability to form non-stoichiometric defective $Ni_{1-x}O$ (Ni^{3+}/Ni^{2+}) powders. Most of the $Ni_{1-x}O$ properties are driven by the level of non-stoichiometry, as exemplified by its electronic conductivity: pure divalent NiO is an intrinsic insulator with a large band gap (>3.5 eV) and very high resistivity ($\rho_{RT} = 10^{13}$ Ω cm) while $Ni_{1-x}O$ is a p-type semi-conductor with ρ_{RT} as low as 10^{-1} Ω cm [16,6]. This motivates and justifies the investigations, such as the present one, aimed at studying the evolution in composition of $Ni_{1-x}O$ samples under specific but mild conditions they can possibly be exposed to during synthetic process or industrial use.

The level of defects in $Ni_{1-x}O$ can be gauged at first glance by the colour of the powder that is green for pure divalent (NiO, Bunsenite), dark olive when slightly oxidized, and black for more oxidized materials containing several percent of Ni^{3+} ($Ni_{1-x}O$) [17]. Structurally, all these phases are commonly described in a face-centred cubic NaCl-type symmetry even if a small trigonal distortion ($\alpha = 60° 4.2'$) appears below its Néel temperature (525 K) [18,19]. It has been reported that this distortion is weaker for

* Corresponding author. Laboratoire de Réactivité et Chimie des Solides, Université de Picardie Jules Verne, CNRS UMR 7314, 33 rue Saint Leu, 80039, Amiens, France.
E-mail address: dominique.larcher@u-picardie.fr (D. Larcher).

http://dx.doi.org/10.1016/j.matchemphys.2016.02.038
0254-0584/

materials synthesized at low temperatures and even fully vanishes for high Ni^{3+} contents [20]. The over-oxidation of NiO creates some Ni^{3+} and Ni vacancies. Reported cubic cell parameter for stoichiometric NiO samples is in the 4.177 Å – 4.178 Å range [21–23].

In the 70's, many groups (e.g. M. Figlarz) explored the relationships between crystallite size, cell parameter and Ni oxidation state in $Ni_{1-x}O$. For samples prepared under air through decomposition/combustion of precursors, the cell parameter of $Ni_{1-x}O$ is found to linearly increase with i) the inverse of the crystallite size (L_c), ii) the amount of Ni^{3+}, iii) the level of structural stress/strain (ε) [21,22]. It turns out that this expansion of the cell parameter, inferred from XRD data, is mainly due to surface relaxation when the crystallite size reaches the nanometric range, as now well documented for many ionic materials [24,25]. Accordingly, pure nanometric stoeichiometric (green) NiO samples prepared without exposure to air have the same cell parameter as oxidized samples having the same crystallite (L_c) size. So, the linear relationship between $\%Ni^{3+}$ and the lattice parameter is not a general rule, but it can be observed for series of samples prepared under air in similar conditions.

Recently, we prepared monodispersed nanometric (few nm) Ni–O particles as model materials for the measurement of interfacial energies via an original and simple potentiometric setup [26]. These powders were prepared by decomposition of Ni^{2+}-oxalate hydrate ($NiC_2O_4 \cdot 2H_2O$) under air (320 °C) reproducibly leading to very small, crystallized and loosely packed oxide particles [27]. Their Ni^{3+} content can be tuned by playing with the dwell time at 320 °C, the $\%Ni^{3+}$ globally decreasing with time. Looking carefully at the parallel evolutions in particle size, structure, texture and chemical composition of these particles along this isothermal heating revealed unexpected features potentially valuable in view of the numerous fields and applications concerned by these materials.

2. Experimental techniques and samples descriptions

A nickel oxalate gel was obtained by adding 50 mL of an ethanol solution of $Ni(NO_3)_2 \cdot 6H_2O$ (0.2 M) to 50 mL of an ethanol solution of $H_2C_2O_4 \cdot 2H_2O$ (1 M) [27]. The resulting green gel was separated from the solution by repeated washings with ethanol and centrifugation steps (6000 rpm, 10 min) and then dried at 80 °C for 6 h. Ni oxides were formed by heat-decomposition of the nickel oxalate ($NiC_2O_4 \cdot 2H_2O$) in air at 320 °C from 40 min to 34 h and labelled as NiO $_{Time}$. This selected temperature (320 °C) is the onset of the decomposition of the anhydrous NiC_2O_4 into NiO as determined by thermal analysis. 40 min is the time necessary to complete this transformation as checked by XRD and Infrared analysis [26].

Phase composition was determined by X-Ray Diffraction (XRD, Bruker D8 diffractometer, CuKα, λ = 1.54056 Å) equipped with a Position Sensitive Detector (PSD). Cell parameters were estimated by the ERACEL software [28]. Crystallite size (L_c) [29] and structural microstrains (= micro-distortions = $\varepsilon = |\Delta d/d|$ with d = interplanar distance) [30] were obtained with the Williamson–Hall method [31] from the positions and FWHM (Full Width at Half Maximum) of five diffraction peaks (111, 200, 220, 311, 222). Dimensionless ε is defined as the slope of the $\beta_{2\theta}.\cos\theta = f(\sin\theta)$ line plot, and L_c is deduced from the intercept value defined as equal to $K_w.\lambda/L_c$. As suggested in the literature for isotropic domains having cubic symmetry [29,32,33], the Scherrer constant (K_w) was fixed equal to 0.90. Specific surface areas were determined using the Brunauer–Emmett–Teller (BET) multipoint method [34] from N_2 physisorption at 77 K (Micromeritics). The nickel mean oxidation state (m.o.s) was determined by iodometric titration. The powder (50 mg) was dissolved in 6 M HCl aqueous solution containing KI excess (500 mg) degassed with N_2 flow. I_2 resulting from the oxidation of iodide by Ni^{3+} was back-titrated with a $Na_2S_2O_3$ solution (10^{-2} M) using starch as end-reaction indicator. The total nickel contents were measured by titration with Na-EDTA and murexide as indicator (absolute incertitude = +/– 0.04). The as-measured percentages of trivalent nickel (100 x Ni^{3+}/Ni_{tot}) perfectly match the values deduced from the cubic cell parameter, as proposed in [21]. This clear linearity is shown in Fig. 1 and enables us to directly infer the level of trivalent nickel in a given sample from its cubic cell parameter.

Thermo-Gravimetric Analysis (TGA) and Differential Scanning Calorimetry (DSC, heat flux calorimeter) were performed under dry-air flow (100 mL/min) on STA449C and DSC204F1 apparatus, respectively. TGA was coupled to a Quadrupole-Mass Spectrometer (MS) (QMS 403 Aëolos). As the temperature is constant, no deviation in weight is expected due to changes in buoyancy.

3. Results and discussion

Our initial sample (NiO_{40min}) is made of monolithic, isotropic and mono-disperse 4 nm particles (see Fig. 2a), containing 7% Ni^{3+} and having a level of micro-strains $\varepsilon = 10^{-3}$ (see Figs. 2b and 3b) [26]. Size and necklace organization of the particles is a memory of the diameter and of the acicular morphology of the oxalate precursor particles, respectively. So, a control of the oxide particles size could be possible through a controlled precipitation of the oxalate precursor [35,36].

During the isothermal air-annealing at 320 °C of this powder, its cubic cell parameter (and related $\%Ni^{3+}$), BET specific surface area,

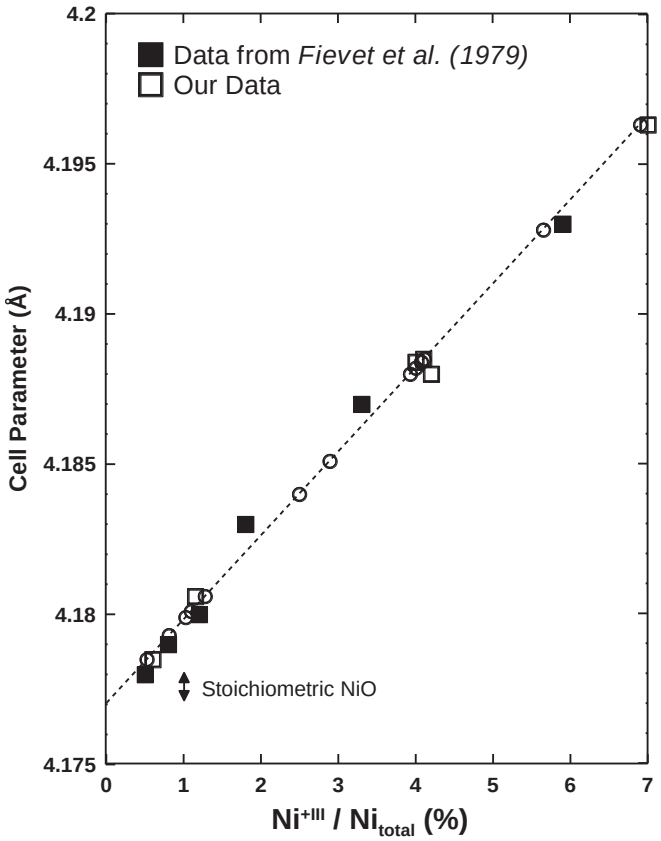

Fig. 1. Correlation between the cubic cell parameter (Å) and the $\%Ni^{3+}$ for various $Ni_{1-x}O$ samples, based on data from [21] (black squares) and our present data (empty squares). Empty circles indicate the samples for which this linearity was used to directly evaluate their $\%Ni^{3+}$ from the cell parameter.

Please cite this article in press as: D. Larcher, et al., Chemical, textural and structural evolution of $Ni_{1-x}O$ nanoparticles upon isothermal air heating, Materials Chemistry and Physics (2016), http://dx.doi.org/10.1016/j.matchemphys.2016.02.038

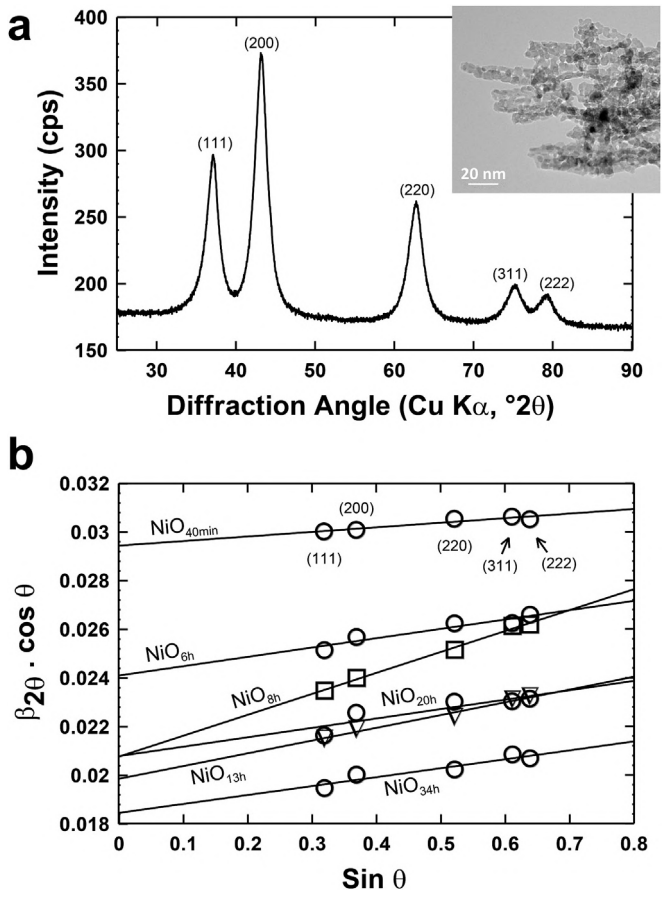

Fig. 2. (a) X-Ray Diffraction pattern and TEM picture for NiO_{40min}, (b) Williamson–Hall plots for selected $Ni_{1-x}O$ samples. According to this formalism, each empty symbol (square, triangle and circle) corresponds to the $\beta_{2\theta}.\cos\theta$ and $\sin\theta$ values deduced from each XRD peak. Each line fits the data collected for each sample (5 peaks). Miller's indexes are also indicated.

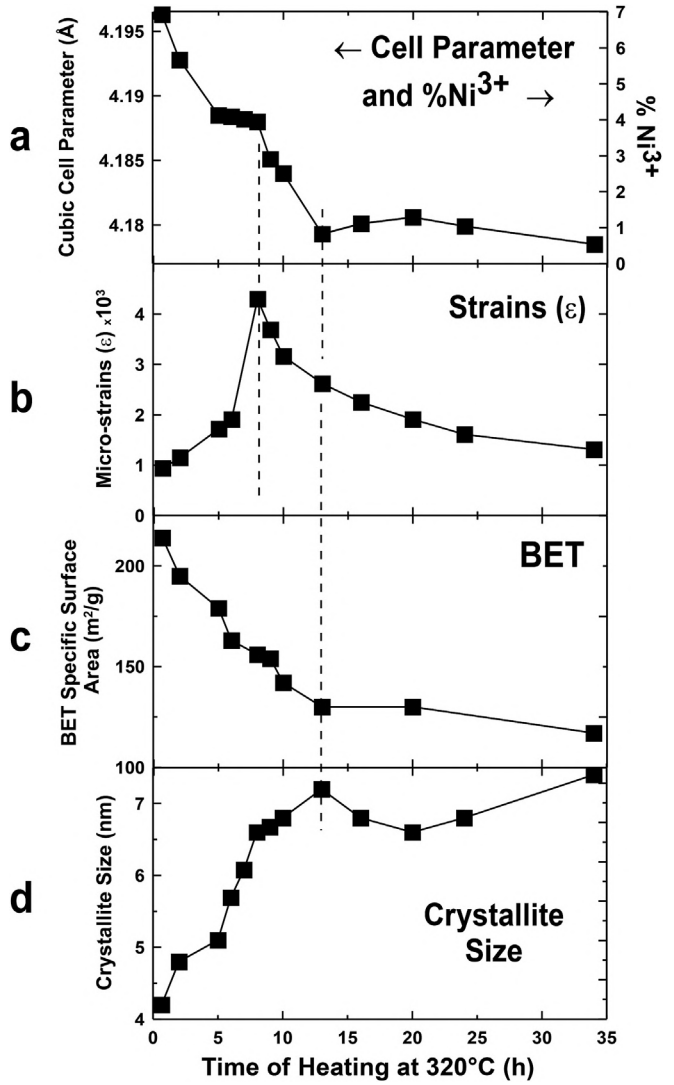

Fig. 3. Evolutions, as function of the heating time of $Ni_{1-x}O$ samples at 320 °C, in (a) cubic cell parameter (and correlated $\%Ni^{3+}$), (b) crystallographic micro-strains (ε), (c) BET specific surface area, and (d) crystallite size. Vertical dashed lines are eye-guides.

crystallite size (L_c) and crystallographic micro-strains (ε) evolve as depicted in Fig. 3. Fig. 2b compares Williamson–Hall plots for NiO_{40min} and some other selected samples.

From NiO_{40min} to NiO_{34h}, the BET specific surface area drops from 215 m^2/g to 120 m^2/g, L_c increases from 4 nm to 7 nm, and TEM observations reveal almost spherical and mono-dispersed domains. All these data consistently indicate that the volume of each NiO_{34h} particle is ca. 5 times larger than that of each NiO_{40min} particle. In other words, each NiO_{34h} particle originates from the sintering of five NiO_{40min} crystals. Our previous investigations [26] revealed that the crystallites size (L_c) perfectly matches the particles size (i.e. monolithic texture) for NiO_{40min} and NiO_{34h}. In contrast, for intermediate samples, L_c values are systematically, though slightly, lower than particle sizes, hinting at a slightly mosaic texture. The very good agreement between the BET specific surface area and the calculated geometrical surface area values (assuming spherical, dense and mono-dispersed crystallite) further suggests that all these powders can be considered as mostly consisting of monolithic domains.

However, during this isotherm, some aspects of the powders are not evolving in a straight manner. Crystallographic strains ε (Figs. 2b and 3b) largely increase from NiO_{40min} ($\varepsilon = 10^{-3}$) to NiO_{8h} ($\varepsilon = 4.3\ 10^{-3}$) then progressively and more slowly drop to nearly go back to the initial value for NiO_{34h} ($\varepsilon = 1.3\ 10^{-3}$). This is a very unusual behaviour since heat-induced sintering generally comes with a monotonous release of these strains as the size increases [21]. The maximum in ε (NiO_{8h}) does not correspond to any clear break or discontinuity in the evolution in BET or in crystallite size, but it corresponds to a plateau in the Ni^{3+} content (~4% Ni^{3+}) (Fig. 3). This can be tentatively understood based on the localization of the excess oxygen, now well established to be preferentially localized at the surface of the particles or within a thin surface shell [37–39]. During the coalescence process, the surface area decreases and excess oxygen therefore has to escape from the grains. We believe that at least a part of the excess surface oxygen of merging particles is trapped in the bulk of the resulting larger particles, hence an increase in structural strains up to a maximum (saturation), NiO_{8h} in our case. The catalytic activity of nanoscale NiO triggered many investigations to decipher the exact nature (adsorbed O_2, surface O^-, structural O^{2-}) of the excess oxygen [38,39]. Albeit still under debate, any of these species can be trapped as above suggested.

Beyond this critical heating time (8 h) and grain size, both excess oxygen and linked crystallographic strains start to be released. While these strains monotonously decrease until the final NiO_{34h} sample (Fig. 3b), it is interesting to note that its crystallite/particle sizes, $\%Ni^{3+}$ and BET values are almost already reached for NiO_{13h}.

Please cite this article in press as: D. Larcher, et al., Chemical, textural and structural evolution of $Ni_{1-x}O$ nanoparticles upon isothermal air heating, Materials Chemistry and Physics (2016), http://dx.doi.org/10.1016/j.matchemphys.2016.02.038

But from NiO_{13h} to NiO_{34h}, the continuous decrease in strains apparently necessitates a temporary gain in oxygen, mirrored by a temporary decrease in crystallite size (Fig. 3a and d). One possible scenario to account for this unexpected behaviour is related to the diffusion of the residual excess oxygen from the bulk towards the surface of these larger grains. This diffusion, whereas having a global relaxation effect onto the entire grain, trigger local changes in vacancy and oxygen concentration that could result in the temporary formation of new crystallite boundaries, with concomitant transient formation of surface Ni^{3+}. Transmission Electron Microscopy coupled with spectral analysis (EELS) is presently underway to localize/visualize this phenomenon.

Our observations were confirmed by thermal analysis that indeed revealed a transient weight gain (TGA) within this range of reaction time, together with a small exothermic heat flow (DSC) (Fig. 4). During this process, the maximum weight gain exactly matches the increase in Ni^{3+} content, assuming oxidation of Ni^{2+} into Ni^{3+} through the incorporation of O^{2-} ions from molecular O_2. The change in Ni^{3+} deduced from the change in lattice constant is unlikely an artefact. No other gaseous product could be detected during this step by MS. In Fig. 4, lattice parameter (%Ni^{3+}) and TGA/DSC signals have been collected in different ways, the former from different samples individually heated for various times then cooled down and analysed, the latter through a dynamic "in-situ" analysis. This can explain the slight time shift between the two sets of data, namely a delayed maximum in weight gain for the thermal data. Before 20 h, the weight evolution is quite difficult to interpret because water production from recombination of surface hydroxyl groups superimposes to O_2 release.

All these observations suggest an intimate link between the textural evolution of $Ni_{1-x}O$ powders and O_2 exchanges with the surrounding, so that changes in O_2 content of the atmosphere should definitively impact the sintering process. Interestingly, this was already experimentally observed for micrometric $Ni_{1-x}O$ with much lower Ni^{3+} contents than nanometric ones [40].

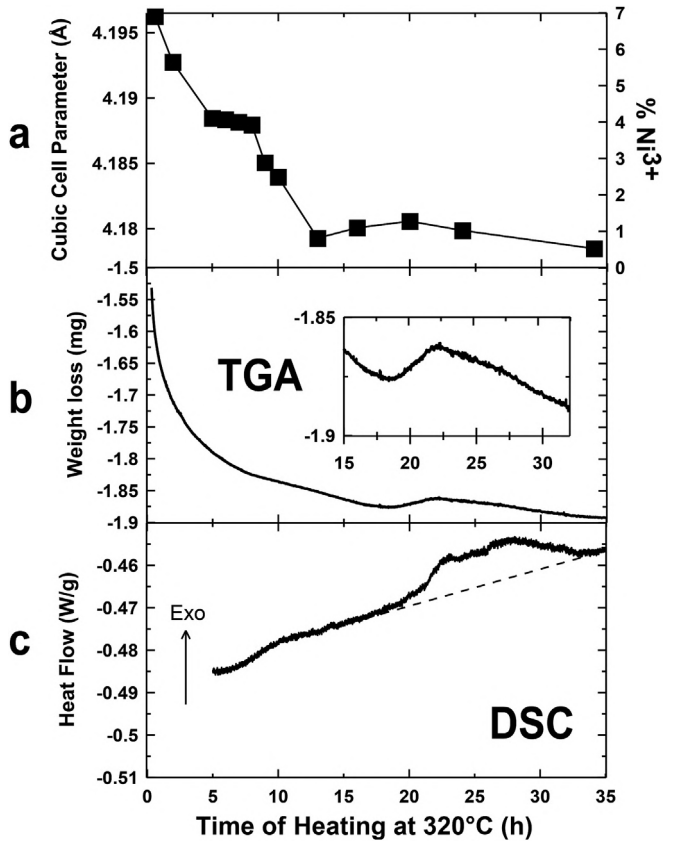

Fig. 4. Comparative evolutions upon heating in (a) %Ni^{3+} (b) weight (TGA trace) and (c) heat exchanges (DSC) for $Ni_{1-x}O$ samples.

4. Conclusions

The chemical, structural and textural evolutions of nanometric monolithic $Ni_{1-x}O$ (~4 nm, 7% Ni^{3+}) particles upon isothermal heating (320 °C) are intimately bound and were found to evolve in unexpected ways, some aspects still remaining to be unravelled. Owing to the wide range of industrial uses and applications devoted to this material, it is worth focussing on the aging and evolution mechanisms using local probing tools, and synthetic works remain to be done in order to explore the possibility of individually tuning the size, composition and texture of this material. In connexion with our previous investigations [26] NiO samples with high levels of strains, whatever their %Ni^{3+}, are those also exhibiting a large excess in surface energy, so expected to be long-term unstable under certain conditions of use/storage.

Such multi-parameter investigation of the stability and evolution of NiO nanoparticles upon aging can be of great interest in critical energy fields. For instance, one can think about implications in applications i) requiring permanent contact of the active nanoparticles with a liquid (e.g. semiconductor in Dye Sensitive Solar Cells or Supercapacitors), ii) involving recurrent temperature shifts (e.g. spectral selective surface for Solar Thermal Collectors), or iii) exposing the particles to cyclic changes in oxygen pressure (metal-air batteries).

Acknowledgements

Authors thank C. Davoisne (LRCS) and S. Bruyère (LRCS) for TEM observations, as well as C. Lenfant (LRCS) for proofreading. French Ministry of Research (MENRT) is acknowledged for its financial support.

References

[1] G.T. Rymer, J.M. Bridges, J.R. Tomlinson, Kinetic and magnetic studies on supported nickel oxide catalysts, J. Phys. Chem. 65 (12) (1951) 2152.
[2] I. Hotovy, J. Huran, P. Siciliano, S. Capone, L. Spiess, V. Rehacek, The influences of preparation parameters on NiO thin film properties for gas-sensing application, Sensors Actuators B Chem. 78 (1–3) (2001) 126.
[3] R. Palombari, Influence of surface acceptor-donor couples on conductivity and other electrochemical properties of nonstoichiometric NiO at 200°C, J. Electroanal. Chem. 546 (23) (2003).
[4] J.S.E.M. Svensson, C.G. Granqvist, Electrochromic hydrated nickel oxide coatings for energy efficient windows: optical properties and coloration mechanism, Appl. Phys. Lett. 49 (1986) 1566.
[5] R. Palombari, F. Pierri, J. Electroanal. Chem. 433 (1997) 213.
[6] H. Sato, T. Minami, S. Takata, T. Yamada, Transparent conducting p-type NiO thin films prepared by magnetron sputtering, Thin Solid Films 236 (1993) 27.
[7] M.P. Proenca, C.T. Sousa, A.M. Pereira, P.B. Tavares, J. Ventura, M. Vazquez, J.P. Araujo, Size and surface effects on the magnetic properties of NiO nanoparticles, Phys. Chem. Chem. Phys. 13 (2011) 9561.
[8] Eric L. Miller, Richard E. Rocheleau, Electrochemical and electrochromic behavior of reactively sputtered nickel oxide, J. Electrochem. Soc. 144 (6) (1997) 1995.
[9] J. He, H. Lindstro1m, A. Hagfeldt, S.-E. Lindquist, Dye-sensitized nanostructured p-type nickel oxide film as a photocathode for a solar cell, J. Phys. Chem. B 103 (1999) 8940.
[10] P. Poizot, S. Laruelle, S. Grugeon, L. Dupont, J.-M. Tarascon, Nano-sized transition-metal oxides as negative-electrode materials for lithium-ion batteries 407 (2000) 496.
[11] K.-C. Liu, M.A. Anderson, Porous nickel oxide/nickel films for electrochemical capacitors, J. Electrochem. Soc. 143 (1) (1996) 124.
[12] V. Srinivasan, J.W. Weidner, An electrochemical route for making porous nickel oxide electrochemical capacitors, J. Electrochem. Soc. 144 (8) (1997) L210.
[13] Se-Hee Lee, C. Edwin Tracy, J. Roland Pitts, Effect of nonstoichiometry of nickel

oxides on their supercapacitor behavior, Electrochem. Solid-State Lett. 7 (10) (2004) A299.
[14] M. Hong, H.C. Choi, H.R. Byon, Nanoporous NiO plates with a unique role for promoted oxidation of carbonate and carboxylate species in the Li–O_2 battery, Chem. Mater. 27 (6) (2015) 2234.
[15] Quang Minh Nguyen, Technological status of nickel oxide cathodes in molten carbonate fuel cells-a review, J. Power Sources 24 (1) (1988) 1.
[16] D. Adler, J. Feinleib, Electrical and optical properties of narrow-band materials, Phys. Rev. B 2 (8) (1970) 3112.
[17] O. Glemser, in: Handbook of Preparative Inorganic Chemistry, second ed. Vol. 2, Academic Press (New-York), 1965, p. 1548.
[18] H.P. Rooksby, A note on the structure of nickel oxide at subnormal and elevated temperatures, Acta Cryst. 1 (1948) 226.
[19] C.J. Toussaint, A high-temperature X-ray diffraction study of the NiO-Li_2O system, J. Appl. Cryst. 4 (1971) 293.
[20] Yasumitsu Shimomura, Ichiro Tsubokawa, Morio Kojima, On nickel oxides of high oxygen content, J. Phys. Soc. Jpn. 9 (1954) 521.
[21] F. Fiévet, P. Germi, F. De Bergevin, M. Figlarz, Lattice parameter, microstrains and non-stoichiometry in NiO. Comparison between mosaic microcrystals and quasi-perfect single microcrystals, J. Appl. Cryst. 12 (1979) 387–394.
[22] F. Fiévet, P. Germi, F. de Bergevin, C. Roger, M. Figlarz, Variation du paramètre cristallin de l'oxyde de nickel à l'état divisé, Mater. Res. Bull. 11 (6) (1976) 681–688.
[23] S. Sasaki, K. Fujino, Y. Takeuchi, X-Ray determination of electron-density distributions in oxides, MgO, MnO, CoO, and NiO, and atomic scattering factors of their constituent atoms, Proc. Jpn. Acad. Ser. B 55 (No. 2) (1979) 43–48.
[24] T.B. Rymer, The lattice constants of small crystals, Suppl. al Nuovo Cimento 6 (Serie X) (1957) 294.
[25] P.J. Anderson, Lattice parameter of finely divided MgO, Mater, Res. Bull 3 (6) (1968) 535.
[26] K. Croué, J.-P. Jolivet, D. Larcher, Direct determination of oxide surface free energy through potentiometric measurements, Electrochem. Solid-State Lett. 15 (1) (2012) F8–F11.
[27] G.J. Li, X.X. Huang, Y. Shi, J.K. Guo, Preparation and characteristics of nanocrystalline NiO by organic solvent method, Mater. Lett. 51 (2001) 325.
[28] J. Laugier, A. Filhol, ERACEL Program, CELREF, 1978.
[29] P. Scherrer, Nach. Ges. Wiss. Gott 2 (1918) 98.
[30] A.R. Stokes, A.J.C. Wilson, The Diffraction of X-rays by distorted crystal aggregates-I, Proc. Phys. Soc. Lond. 56 (1944) 174.
[31] G.K. Williamson, W.H. Hall, X-Ray line broadening from filed aluminium and wolfram, Acta Metall. Mater. 1 (1953) 22.
[32] J.I. Langford, A.J.C. Wilson, Scherrer after sixty years: a survey and some new results in the determination of crystallite size, J. Appl. Cryst. 11 (1978) 102–113.
[33] H.P. Klug, L.E. Alexander, X-ray Diffraction Procedures for Polycrystalline and Amorphous Materials, second ed., Wiley, New York, 1974.
[34] S. Brunauer, P.H. Emmett, E. Teller, J. Am. Chem. Soc. 60 (1938) 309.
[35] J.A. Allen, The precipitation of nickel oxalate, J. Phys. Chem. 57 (7) (1953) 715.
[36] J.A. Allen, C.J. Haigh, The surface area of nickel oxalate precipitates, J. Am. Chem. Soc. 76 (20) (1954) 5245.
[37] T. Uchijima, M. Takahashi, Y. Yoneda, The measurement of surface excess oxygen of nickel oxide catalysts by reduction with hydrazine, Bull. Chem. Soc. Jpn. 4 (1967) 2767.
[38] A. Bielanski, M. Najbar, Adsorption species of oxygen on the surfaces of transition metal oxides, J. Catal. 25 (1972) 398.
[39] J. Deren, J. Stoch, Effect of biography on stoichiometric composition and chemisorptive properties of nickel oxide (Oxygen Chemisorption), J. Catal. 18 (1970) 249.
[40] S.B. Boskovic, M. Ristic, Sintering of nonstoichiometric nickel oxide, Poroshkovaya Metall. 9 (117) (1972) 88.

Please cite this article in press as: D. Larcher, et al., Chemical, textural and structural evolution of $Ni_{1-x}O$ nanoparticles upon isothermal air heating, Materials Chemistry and Physics (2016), http://dx.doi.org/10.1016/j.matchemphys.2016.02.038